Single-phonon scattering from clean flat metal surfaces

2002 J. Phys.: Condens. Matter 14 5881

(http://iopscience.iop.org/0953-8984/14/24/302)

INSTITUTE OF PHYSICS PUBLISHING JOURNAL OF PHYSICS: CONDENSED MATTER

J. Phys.: Condens. Matter **14** (2002) 5881–5901 PII: S0953-8984(02)34877-X

Single-phonon scattering from clean flat metal surfaces

A Franchini and G Santoro

Dipartimento di Fisica dell' Università di Modena e Reggio Emilia e Istituto Nazionale di Fisica della Materia—Unità di Modena, Via Campi 213/A, 41100 Modena, Italy

Received 14 March 2002
Published 31 May 2002
Online at stacks.iop.org/JPhysCM/14/5881

Abstract

In this paper we review the recent advances of the He atom scattering experiments and the theoretical interpretation of the time-of-flight (TOF) spectra relative to clean flat metal surfaces in the one-phonon regime. We discuss the atom–surface scattering mechanism, including the anomalies in the metal surface phonon spectrum and the details of the atom–surface interaction potential. In particular we focus the discussion on the anticorrugating effects in the TOF intensities.

1. Introduction

Atom surface scattering experiments started around 1930 with the experiments performed by Stern [1]. In the same period atom surface scattering theory was developed by Jackson and Mott [2]. However the real breakthrough took place only in the 1960s with the development of high-vacuum systems and of the supersonic beam technique, which provide intense and almost monochromatic He atom beams (HAS technique) [3,4]. From the theoretical side the advances were made possible by the development of fast computers to solve the quantum mechanical problem for realistic models. In the book *Dynamics of Gas Surface Interaction* [5], many experimental and theoretical aspects of the problem are discussed. Earlier reviews covering part of this subject are those of Goodmann and Wachmann [6], Engel and Rieder [7], Toennies [8], Celli [9], Barker and Auerbach [10], Bortolani and Levi [11] and Gumhalter [12].

The first evidence of the dispersion relation for the Rayleigh surface phonons along the whole surface Brillouin zone was achieved [13, 14] by using the HAS technique for LiF. This method has been applied to the study of other alkali halides [15, 16], semiconductors [17–20] and metals [21–31].

The HAS spectroscopy gives phonon dispersion curves on surfaces with accuracy comparable to that realized in the neutron inelastic scattering studies of bulk crystals. The inelastic He scattering method offers impressively high resolution in the range of 0.1 meV. This allows the study of the systematics of surface phonons, including the linewidth. Helium atoms are believed, to an excellent approximation, to sample only the motion of atoms in the outermost atomic layer.

The atom scattering is better in the determination of modes having energy below 20–30 meV: the region of energy of the surface phonons for many metals. If the energy exchanged by the He atom with the surface exceeds this limit, multi-phonon processes take place, washing away the details of the surface lattice dynamics.

In this review we focus on the theoretical interpretation of time-of-flight (TOF) experiments from clean and unreconstructed metal surfaces. The paper is organized as follows.

In section 2 we introduce useful notations and the kinematics of the He atom surface scattering, by focusing on the importance of in-plane scattering.

In the subsequent section 3 we discuss at some length the theory of the He atom scattering in the framework of the two potentials of Gell-Man and Goldberger [32]. We show the convenience of choosing the 'large potential' as the laterally averaged atom–surface potential, which gives rise to specular reflection only. With this choice to lowest order in the scattering matrix T we derive a formula for the reflection coefficient in the distorted Born approximation (DWBA) [33].

The derivation of the He–surface potential is discussed in the subsequent section 4. Because even in the present day a detailed calculation of the He–surface potential cannot be performed with the same accuracy for all the distances of the He atom from the surface, we split this interaction into a repulsive interaction valid at small distances of the He atom from the surface and an attractive part dominated by van der Waals forces at large distances of the He atom from the surface. We also discuss the smoothing of the van der Waals interaction in the region of close approach of the He atom to the surface (3–4 Å), which is of crucial interest. At the end of the section we introduce the effects of the anticorrugation of the atom–surface potential in the evaluation of the differential reflection coefficient.

The problem of the determination of surface phonons is presented in section 5, where we present the phenomenological models and the recent models obtained at least for simple metals in a fully microscopic self-consistent approach.

Finally section 6 is devoted to the comparison of the theoretical calculations with the experiments for simple, noble and transition metal surfaces.

2. Atom–surface interaction kinematics

In order to analyse the experimental data of TOF spectra obtained with a molecular beam apparatus we shall first discuss the kinematical theory of the scattering.

The crystal lies in the $z < 0$ region, where z is the axis normal to the mean plane of the surface. ϵ_i is the energy of the He atom impinging on the surface in the direction defined by the polar and azimuthal angles θ_i and φ_i, and ϵ_f is the energy of the atom reflected in the direction defined by the polar and azimuthal angles θ_f and φ_f. The scattering geometry is drawn in figure 1. The incident He atom wavevector is denoted by $\vec{k}_i = (\vec{K}_i, k_{iz})$, where $\vec{K}_i$ is the wavevector component parallel to the surface and k_{iz} is the component perpendicular to the surface, while for the scattered He atom the wavevector is $\vec{k}_f = (\vec{K}_f, k_{fz})$. Because the incident and reflected He atoms are free particles the incident and scattered energies are

$$\epsilon_i = \frac{\hbar^2 k_i^2}{2m} \qquad \epsilon_f = \frac{\hbar^2 k_f^2}{2m} \tag{1}$$

where m is the He atom mass. In the one-phonon regime with in-plane scattering conditions the initial momentum of the He atom parallel to the surface $\vec{K}_i$ and the final momentum $\vec{K}_f$ must fulfill the lateral momentum conservation law

$$\vec{K}_f - \vec{K}_i = \vec{Q} + \vec{G} \tag{2}$$

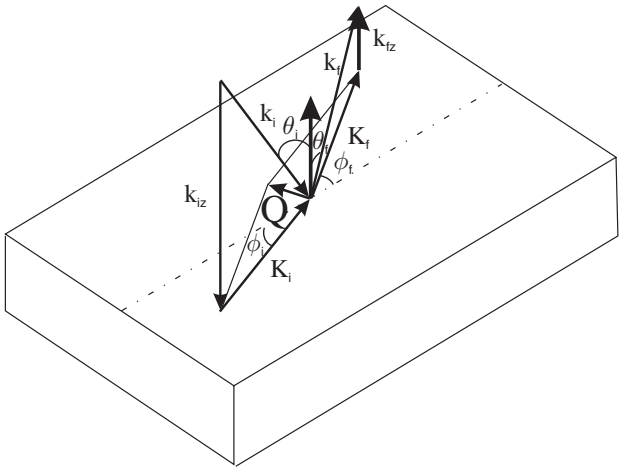

Figure 1. He surface scattering geometry. Q is the wavevector of a surface phonon.

where $\vec{Q}$ is the momentum of the phonon and $\vec{G}$ is a vector of the reciprocal lattice of the surface, while the energy of the He beam must fulfill the energy conservation law

$$\epsilon_f - \epsilon_i = \pm\hbar\omega(\vec{Q}) \tag{3}$$

where $\omega(\vec{Q})$ is the frequency of the phonon. The sign + refers to the annihilation events, while the sign − refers to creation events.

The simultaneous conservation of energy and momentum gives

$$\hbar\omega(\vec{Q}) = \pm\frac{\hbar^2\{K_i^2[1 - (\sin^2\theta_f)/(\sin^2\theta_i)] + 2\vec{K}_i\cdot(\vec{Q}+\vec{G}) + |\vec{Q}+\vec{G}|^2\}}{2m\sin^2\theta_f}. \tag{4}$$

The rhs of equation (4) is usually called the 'scan curve' of the experiment. As one can see from equation (4), in inelastic one-phonon scattering events only those phonon modes corresponding to the intersections between the scan curve and the phonon dispersion relation are observed.

3. Inelastic scattering theory

Since we are interested in low-energy atom–surface scattering in which the incoming particles do not penetrate into the surface, following the two-potential formalism of Gell-Mann and Goldberger [32] the total interaction potential V_i is divided into a large part U exhibiting total specular reflection and diffraction and a remainder $v = V_i - U$, which must be treated approximately. The potential U is the laterally average (hereafter defined) of the total potential with the assumption that all the ions of the crystal are in their equilibrium positions.

The interaction potential V_i can be written as a sum of pairwise atomic potentials

$$V_i = \sum_{l,\kappa} v_a(\vec{r} - \vec{r}_{l\kappa} - \vec{u}_{l\kappa}) \tag{5}$$

where $\vec{r}$ is the position of the He atom, $\vec{r}_{l\kappa} = (\vec{R}_l + \vec{R}_\kappa, z_\kappa)$ is the equilibrium position of crystal atoms and $\vec{u}_{l\kappa}$ is their displacement from equilibrium positions. The laterally averaged potential can be written as

$$U(z) = \frac{1}{NA_c}\int_{surface} \mathrm{d}^2\vec{R} \sum_{l,\kappa} v_a(\vec{R} - \vec{R}_l - \vec{R}_\kappa, z - z_\kappa) = \sum_\kappa \frac{1}{A_c}\int_{surface} \mathrm{d}^2\vec{R}\, v_a(\vec{R}, z - z_\kappa) \tag{6}$$

where N is the number of unit cells of area A_c.

The eigenfunctions of U corresponding to outgoing (+) and incoming (−) wave boundary conditions are denoted by $\chi_r^{(\pm)}$; they are products of a vibrational wavefunction for the solid, a plane wave for the particle motion parallel to the surface and a wavefunction $\chi^{(\pm)}(k_{rz}, z)$ for particle motion in the z direction, which obeys the equation

$$\left(\frac{\hbar^2}{2m}\frac{\partial^2}{\partial z^2} + \frac{\hbar^2 k_{rz}^2}{2m} - U\right)\chi_r^{(\pm)}(k_{rz}, z) = 0 \qquad r = i,\ f. \tag{7}$$

Here the subscripts i (initial state) and f (final state) are collective indices for the wavevector $(\vec{K}, k_z)$ of the particle and the number of phonons $\{n\}$ in each vibrational mode of the crystal. Equation (7) can have solutions for $k_{rz}^2 < 0$ corresponding to surface bound states.

The transition rate w_{fi} from the initial state i to the final state f is given in terms of the transition matrix T_{fi} by

$$w_{fi} = \frac{2\pi}{\hbar}|T_{fi}|^2\delta(E_i - E_f) \tag{8}$$

where E_f and E_i are the final and initial energies for the whole system.

Gell-Mann and Goldberger [32] have shown that the matrix elements T_{fi} are equivalent to

$$T_{fi} = (\phi_f|T|\phi_i) = (\phi_f, U\chi_i^{(\pm)}) + t_{fi} \tag{9}$$

where ϕ_f and ϕ_i describe the final and initial wavefunctions of the unperturbed system and t_{fi} is given by

$$t_{fi} = (\chi_f^{(-)}, v\chi_i^{(+)}) + \sum_c (\chi_f^{(-)}, v\chi_i^{(-)})\frac{t_{ci}}{E_i - E_c}. \tag{10}$$

The matrix element t_{fi} contains all the information about the inelastic scattering through the potential v.

The reflection coefficient $R(k_f, k_i)$ is obtained by dividing the transition rate by the initial particle flux $j_i = \hbar k_{iz}/mL_z$, summing over all phonon states and averaging over all initial states

$$R(k_f, k_i) = \frac{1}{j_i}\sum_{\{n_f\}}\sum_{\{n_i\}} \rho(\{n_i\})w_{fi} \tag{11}$$

where $\rho(\{n_i\})$ is the distribution of initial phonon states. For inelastic scattering the measured quantity is the differential scattered intensity $\mathrm{d}R/\mathrm{d}k_f^3$. This is obtained upon multiplying the reflection coefficient defined in equation (11) by the available volume in the phase space $L_z L_c^2/(2\pi)^3$ for the scattered particle. By using $\mathrm{d}^3k_f = k_f^2\,\mathrm{d}k_f\,\mathrm{d}\Omega_f$ and equation (1) we find

$$\frac{\mathrm{d}^2R}{\mathrm{d}E_f\,\mathrm{d}\Omega_f} = \frac{L_z L_c^2}{(2\pi)^3}\frac{|k_f|m}{\hbar^2}R(k_f, k_i). \tag{12}$$

The simplest approximation of equation (12) is the DWBA, obtained by replacing t_{fi} by $v_{fi} = (\chi_f^{(-)}, v\chi_i^{(+)})$. The reflection coefficient for particles scattered from the initial state k_i to the final state k_f is then

$$R(k_f, k_i) = \frac{2\pi}{\hbar j_i}\sum_{\{n_f\}}\sum_{\{n_i\}} \rho(\{n_i\})|(\chi_f^{(-)}, V_i\chi_i^{(+)})|^2\delta(E_f - E_i). \tag{13}$$

Only if a single phonon is exchanged are the conservation of energy (equation (3)) and of the lateral momentum (equation (2)) uniquely satisfied. The one-phonon processes give rise to sharp peaks in the reflection coefficients that are easily identified in the experimental spectra.

We need t_{fi} to first order in the displacements $\vec{u}_{l\kappa}$ of the atoms of the crystal from their equilibrium positions. In the harmonic approximation the displacement $\vec{u}_{l\kappa}$ of an atom of the crystal can be expanded in normal modes as follows:

$$\vec{u}_{l\kappa} = \left(\frac{\hbar}{NM_\kappa}\right)^{1/2} \sum_{\vec{Q},j} \left(\frac{1}{2\omega(\vec{Q},j)}\right)^{1/2} \vec{e}_\kappa(\vec{Q},j)\left[a(\vec{Q},j) + a^\dagger(-\vec{Q},j)\right] e^{i\vec{Q}\cdot(\vec{R}_l+\vec{R}_\kappa)} e^{-i\hbar\omega(\vec{Q},j)} \tag{14}$$

where $a(\vec{Q},j)$ and $a^\dagger(-\vec{Q},j)$ are the usual annihilation and creation operators, M_κ is the mass of the κth lattice ion of the basis and $\vec{e}_\kappa(\vec{Q},j)$ is the polarization vector of the jth normal mode normalized such that

$$\sum_\kappa \vec{e}^{\,*}_\kappa(\vec{Q},j)\vec{e}_\kappa(\vec{Q},j') = \delta_{jj'}. \tag{15}$$

We expand the surface–atom interaction potential $V_i(\vec{r},\{\vec{u}\})$ to first order in the displacements $\vec{u}_{l\kappa}$ as follows:

$$V_i(\vec{r},\{\vec{u}\}) = V_{i0}(\vec{r}) + \sum_{l\kappa} \vec{u}_{l\kappa}\cdot[\nabla_{l\kappa} V_i(\vec{r},\{\vec{u}\})]_{eq} \tag{16}$$

where $V_{i0}(\vec{r}) = [V_i(\vec{r},\{\vec{u}\})]_{eq}$ is the potential at equilibrium and the gradient $\nabla_{l\kappa}$ is performed with respect to the atomic displacements $\vec{u}_{l\kappa}$.

Recalling that we have assumed that V_i is the sum of two-body potentials that depend only on the separation between the position $\vec{r}$ of the He atom and the actual positions of the atoms in the crystal we can write equation (16) in the form

$$V_i(\vec{r},\{\vec{u}\}) = V_{i0}(\vec{r}) - \sum_{l\kappa} \vec{u}_{l\kappa}\cdot\vec{F}_{l\kappa} \tag{17}$$

where $\vec{F}_{l\kappa} = -[\nabla_{l\kappa} v_a(\vec{r}-\vec{r}_l-\vec{r}_\kappa-\vec{u}_{l\kappa})]_{eq}$ is the force exerted by the crystal atom $l\kappa$ on the He atom.

The thermal average of the transition rate results in

$$\langle w_{fi}\rangle = 2\pi \sum_{\vec{Q},j} \frac{n[\omega(\vec{Q},j)]}{2NM_\kappa\omega(\vec{Q},j)} |M_{fi}|^2 \delta(\epsilon_f - \epsilon_i - \hbar\omega(\vec{Q},j)) \tag{18}$$

where

$$M_{fi} = \int d^3\vec{r}\, \chi_f^{(-)*}(\vec{r}) \left[\sum_{l\kappa} \vec{e}_\kappa(\vec{Q},j) e^{i\vec{Q}\cdot\vec{R}_l}\cdot\vec{F}_{l\kappa}(\vec{r})\right] \chi_i^{(+)}(\vec{r}). \tag{19}$$

With our convention on the sign of ω, $\delta(\epsilon_f-\epsilon_i-\hbar\omega(\vec{Q},j))$ automatically picks up the + sign for absorption and the − sign for emission of one single phonon.

For the laterally averaged potential the wavefunctions have the form

$$\begin{aligned} \chi_i^{(+)}(\vec{r}) &= \frac{\chi_i(k_{iz},z)}{(L_c^2 L_z)^{1/2}} e^{i\vec{K}_i\cdot\vec{R}} \\ \chi_f^{(-)}(\vec{r}) &= \frac{\chi_f(k_{fz},z)}{(L_c^2 L_z)^{1/2}} e^{i\vec{K}_f\cdot\vec{R}} \end{aligned} \tag{20}$$

where the wavefunctions are normalized in a box of base area L_c^2 and height L_z.

We can now give an explicit expression for the matrix element M_{fi} (equation (19)) by inserting the $\chi_i^{(+)}$ and $\chi_f^{(-)}$ defined in equation (20) and performing the in-plane integral and the summation. We obtain

$$M_{fi} = \frac{(2\pi)^2}{L_c^2 L_z} \sum_{\vec{G},\kappa} \int \chi_f^*(k_{fz}, z)\vec{e}_\kappa(\vec{Q}, j) \cdot \vec{F}_\kappa(\vec{Q} + \vec{G}, z)\chi_i(k_{iz}, z)\, \mathrm{d}z\, \delta(\vec{K}_f - \vec{K}_i - \vec{Q} - \vec{G}) \tag{21}$$

with

$$\vec{F}_\kappa(\vec{Q} + \vec{G}, z) = -\left(\mathrm{i}(\vec{Q} + \vec{G}), \frac{\partial}{\partial z}\right) v_a(\vec{Q} + \vec{G}, z - z_\kappa)\mathrm{e}^{\mathrm{i}(\vec{Q}+\vec{G})\cdot\vec{r}_\kappa} \tag{22}$$

and

$$v_a(\vec{Q}, z) = \frac{1}{A_c} \int_{surface} \mathrm{e}^{-\mathrm{i}\vec{Q}\cdot\vec{R}} v_a(\vec{r})\, \mathrm{d}^2\vec{R}. \tag{23}$$

We also define

$$\vec{F}_\kappa(\vec{k}_i, \vec{k}_f) = \int \mathrm{d}z\, \chi_f^*(k_{fz}, z)\vec{F}_\kappa(\vec{Q} + \vec{G}, z)\chi_i(k_{iz}, z) \tag{24}$$

to obtain

$$|M_{fi}|^2 = \frac{(2\pi)^2}{L_c^2 L_z^2} \sum_{\vec{G}} \left| \sum_\kappa e_\kappa(\vec{Q}, j) \cdot \vec{F}_\kappa(\vec{k}_f, \vec{k}_i) \right|^2 \delta(\vec{K}_f - \vec{K}_i - \vec{Q} - \vec{G}). \tag{25}$$

From the transition rate equation (18) we obtain by using equation (12) the differential reflection coefficient

$$\frac{\mathrm{d}^2 R}{\mathrm{d}\epsilon_f \mathrm{d}\Omega_f} = \frac{m^2|k_f|}{2N\hbar^3 k_{iz}} \sum_{\vec{Q},\vec{G}} \sum_j \frac{n[\omega(\vec{Q}, j)]}{\omega(\vec{Q}, j)} \delta(\epsilon_f - \epsilon_i - \hbar\omega(\vec{Q}, j)) \times \delta(\vec{K}_f - \vec{K}_i - \vec{Q} - \vec{G}) \left| \sum_\kappa \frac{e_\kappa(\vec{Q}, j)}{\sqrt{M_\kappa}} \cdot \vec{F}_\kappa(\vec{k}_f, \vec{k}_i) \right|^2. \tag{26}$$

The dominant contribution to equation (26) originates from the outermost top layer. The differential reflection coefficient, considering only the scattering from the outermost layer ($\kappa = 0$) and the $\vec{G} = \vec{0}$ term, takes the form

$$\frac{\mathrm{d}^2 R}{\mathrm{d}\epsilon_f \mathrm{d}\Omega_f} = \frac{m^2|k_f|}{2N\hbar^3 k_{iz}} \sum_{\vec{Q},j} \frac{n[\omega(\vec{Q}, j)]}{\omega(\vec{Q}, j)} \delta(\epsilon_f - \epsilon_i - \hbar\omega(\vec{Q}, j))\delta(\vec{K}_f - \vec{K}_i - \vec{Q}) \times \left| \frac{e_0(\vec{Q}, j)}{\sqrt{M_0}} \cdot \int \mathrm{d}z\, \chi_f^*(k_{fz}, z)\left(\mathrm{i}\vec{Q}, \frac{\partial}{\partial z}\right) v_a(\vec{Q}, z)\chi_i(k_{iz}, z) \right|^2. \tag{27}$$

4. The atom–surface potential

In the previous section we derived the one-phonon reflection coefficient in terms of the laterally averaged static potential $U(z)$ and of the force $\vec{F}_{l\kappa}$ between the He atom and the surface atom located at $\vec{r}_{l\kappa}$. For the two-body interactions the potential is well defined in the asymptotic region ($z \to \infty$) and near to the ions, where the closed-shell orbitals of the He atom overlap the surface atom wavefunctions outside the crystal. In the intermediate region the potential is not very well known.

We are then forced to divide the interaction potential into a repulsive part (close to the ions) and an attractive part due to the van der Waals forces [34]. The reduction of the attraction of the van der Waals forces close to the surface is provided by semiempirical (SE) models [35].

It has been shown [36–41] that as a good approximation the repulsive part V_R of the potential can be written as

$$V_R = \alpha\rho(\vec{r}). \tag{28}$$

For metal surfaces the value of the constant α depends on the approach used. Esbjerg and Norskov [41] were the first to obtain equation (28) for a He atom embedded in an homogeneous electron gas with a positive uniform background. The value of α ranges from 305 to 329 eV a_B^3.

Hartree–Fock calculations [42] for the He interacting with a metal atom cluster give $\alpha = 373$ eV a_B^3. Harris and Liebsch [43] by using perturbation theory and treating the He atom outside the crystal as a perturbation of the surface electrons found $\alpha = 500$ eV a_B^3. A similar value has been obtained by the recent more refined calculations of Takada and Kohn [40].

In conclusion the values of α range from 250 to 500 eV a_B^3. Since α is very large the equipotential surfaces which are of interest for the He atom scattering (20–30 meV) corresponds to very low electron densities. This means that in a collision with a metal surface the He atom is reflected back very far from the surface. Typically the classical turning point or the closest impact distance is about 3–4 Å from the surface atoms. At such large distance, the electronic density is very well represented by superimposing the electron densities of the individual atoms. With this superimposition V_R is given by

$$V_R(\vec{r}) = \alpha \sum_{l\kappa} \rho_\kappa(\vec{r} - \vec{r}_{l\kappa}) \tag{29}$$

where the ρ_κ are the atomic charges. Calculations performed with atomic wavefunctions [42] obtained with different degrees of approximation show that the corrugation profile around the classical turning point can be very well approximated by an atomic charge of the type $\bar{\rho}e^{-\beta\vec{r}}$, where $\bar{\rho}$ is a suitable constant and β ranges from 2 to 3 Å^{-1}.

Around the classical turning point z_t we can write

$$V_R(\vec{R}, z) = \alpha\bar{\rho} \sum_{l\kappa} e^{-\beta[(\vec{R}-\vec{R}_l-\vec{R}_\kappa)^2+(z-z_\kappa)^2]^{1/2}}. \tag{30}$$

This formula shows that the main contribution originates from the atoms of the first layer, for which $z_\kappa = 0$. We then consider only the surface layer. This dominant term can be conveniently approximated, since $z_t \gg |\vec{R} - \vec{R}_l|$, by

$$[(\vec{R} - \vec{R}_l)^2 + z^2]^{1/2} \simeq z\left(1 + \frac{(\vec{R} - \vec{R}_l)^2}{2z^2}\right) \simeq z + \frac{(\vec{R} - \vec{R}_l)^2}{2z_t}. \tag{31}$$

The repulsive potential can then be written as

$$V_R(\vec{R}, z) = \alpha\bar{\rho}e^{-\beta z} \sum_l e^{\frac{-\beta(\vec{R}-\vec{R}_l)^2}{2z_t}}. \tag{32}$$

Equation (32) reproduces very well the corrugation obtained by sophisticated self-consistent calculations. The laterally averaged potential corresponding to V_R can be analytically determined as $U_R e^{-\beta z}$, where $U_R = (2\pi z_t/\beta)\alpha\bar{\rho}$.

The attractive interaction arises from the interaction between the electrons of the closed shells of the He atom and the electronic charge profile at the surface of the metal. If one

considers a dipole–dipole interaction the attractive potential at large distances z from the surface has the form

$$V_A = -C_3 \frac{1}{z^3}. \tag{33}$$

The value of C_3 is given by the Lifshitz [44] formula

$$C_3 = \frac{\hbar}{4\pi} \int_0^\infty \mathrm{d}\omega \, \frac{\epsilon(\mathrm{i}\omega) - 1}{\epsilon(\mathrm{i}\omega) + 1} \alpha_{\mathrm{He}}(\mathrm{i}\omega) \tag{34}$$

where ϵ is the dielectric function of the metal surface and α_{He} is the He atom polarizability.

A simple way of determining equation (33) is to sum pairwise dipole–dipole interactions [44]

$$-C_6 \frac{1}{|\vec{r} - \vec{r}_{lk}|^6} \tag{35}$$

where

$$C_6 = \frac{3\hbar}{\pi} \int_0^\infty \alpha(\mathrm{i}\omega)\alpha_{\mathrm{He}}(\mathrm{i}\omega) \, \mathrm{d}\omega \tag{36}$$

where $\alpha(\mathrm{i}\omega)$ is the electronic polarizability of the metal atom. The sum of the terms in equation (35) over an atomic plane of a Bravais lattice and over the equally spaced parallel atomic planes gives

$$V_A = \frac{\pi}{6A_c d} C_6 \frac{1}{(z - d/2)^3} \tag{37}$$

where d is the interplanar spacing.

In the limit of low electronic densities we have

$$C_3 = \frac{\pi}{6A_c d} C_6. \tag{38}$$

Zaremba and Kohn [45–47] derived a similar expression based on the jellium model

$$V_A = -\frac{C_3}{(z - z_{VdW})^3}. \tag{39}$$

They give z_{VdW} for various metallic surfaces. A later paper by Harris and Liebsch [43] suggested that the exact value of z_{VdW} is much closer to the jellium edge $z = d/2$ than Zaremba–Kohn values. Improvements in this formula have been obtained by considering the quadrupole charge fluctuations of the He atom and of the surface electrons. These high-order corrections give the following expression for the van der Waals interaction:

$$V_A(z) = -\frac{C_3}{(z - z_{VdW})^3} - \frac{C_5}{(z - z_{VdW})^5}. \tag{40}$$

The C_5 term has been evaluated explicitly for a local dielectric function [48]. The results presented so far neglect the surface periodicity. Hill *et al* [49] by considering the atom–atom dipole interaction and summing over the lattice sites of a semi-infinite crystal obtained

$$V_A(z) = -\frac{C_3}{(z - d/2)^3} + C' \sum_{\vec{G} \neq \vec{0}} \left(\frac{G}{2z} \right)^2 \mathrm{e}^{\mathrm{i}\vec{G}\cdot\vec{R}} K_2(Gz) \tag{41}$$

where $K_2(Gz)$ is a modified Bessel function. C' is not well known but it can be fitted to the asymptotic behaviour given by equation (39). This is a possible procedure to include the corrugation in the van der Waals attraction.

The major correction that should be included in $V_A(z)$ is at small separation of the He atom from the surface, where the van der Waals interaction diverges. The effect of the charge

overlap is to reduce the attraction strongly at close range and to move the classical turning point closer to the surface, where the variation of the charge density is greater. To eliminate or reduce the effects arising from the unphysical divergence various methods have been proposed. These methods are based on the fact that in the case of atom–atom scattering the van der Waals interaction goes to zero at small separation. The reduction of the pairwise interaction between atoms is well described by the Tang–Toennies [35] damping factor

$$V_A(z) = -\frac{C_6}{z^6} f_6(z) \tag{42}$$

where

$$f_n(z) = 1 - \mathrm{e}^{-\beta z} \sum_{\kappa=1}^{n} \frac{(\beta z)^\kappa}{\kappa!}. \tag{43}$$

The quantity β is the same parameter that describes the falling off of V_R.

In conclusion, the atom–surface van der Waals interaction can be approximated by

$$V_A(z) = -\frac{C_3}{(z - z_{VdW})^3} f_3(z - z_{VdW}). \tag{44}$$

A similar damping factor has been obtained by Norlander and Harris [38] with a pseudopotential (PP) approach. They show that when the cancellation of V_R and V_A is very strong in the region close to the turning point, the presence of the smoothing factor is important in order to obtain a dominant repulsive potential at small z. The f_3 function that they found has the form

$$f_3(x) = 1 - [2x(1 + x) + 1]\mathrm{e}^{-2x} \tag{45}$$

with $x = K_0(z - z_{VdW})$ and K_0 of the order of the inverse atomic radius. The value of K_0 and C_3 determine the well depth.

The total potential is obtained by adding to the repulsive part V_R one of the approximate expressions for the attractive part that we have presented in this section. A typical laterally averaged atom–surface potential is shown in figure 2 for the Ag case.

The construction of the potential is particularly simple if one assumes that the surface charge density is given by a superposition of atomic charge densities. However, He scattering experiments from metal surfaces show that this procedure gives rise to some inconsistency [40, 50–52]. The main problem is that, if the pairwise interactions are adjusted in such a way that the laterally averaged potential reproduces the He bound-state spectrum, the surface corrugation, evaluated with the same potential, is substantially larger than that obtained from the He diffraction patterns [50, 51].

He scattering data indicate that the surface electron density is intrinsically smoothed with respect to the superposition of atomic densities. Recently in elastic scattering studies Rieder and coworkers [53] have found unexpected differences in the corrugations measured with He and Ne atoms. For Rh(110) and Ni(110) these authors conclude that the Ne diffraction data reflect the corrugation of the unperturbed surface, whereas for He atoms they conclude that the corrugation is shifted away from the atomic positions. In other words, with the He scattering at fixed energy, the classical turning point is higher at the bridge position than that for the on-top position. Rieder and Garcia [54] applied the Esbjerg–Norskov approach to study their measurements for Rh(110) and they found that the corrugation is much larger than the experimental one. Annett and Haydock [55] tried to reconcile this disagreement by introducing an extra term into the interaction, called the anticorrugation term, which arises from the hybridization of the He 1s occupied orbital and the empty states of the metal. This hybridization term gives rise to an attractive contribution to the potential, which is stronger in the top positions than in the bridge positions.

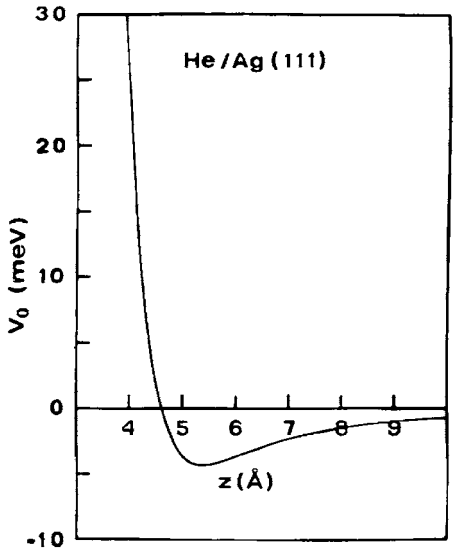

Figure 2. He–Ag(111) laterally averaged potential.

A theoretical explanation based on the density functional approach for Rh(110) has been given by Petersen *et al* [56]. For Rh(110) the electronic states which are more important at the turning point distance have d_{xz} character and cross the Fermi level at the zone boundary. These orbitals change phase in passing from one atom to the next neighbour. At the short bridge position their electron density is high. A He atom, in its 1s state, feels a repulsion from those d_{xz} states and is efficiently reflected. On the other hand the the $2p_x$ and $2p_y$ states of Ne are antisymmetric, so they do not interact with the d_{xz} band. For this reason the authors conclude, in agreement with Rieder's results, that for He at the energy used in the experiments (20–50 meV) the He turning point above the on-top position is closer to the surface than that above the short-bridge position. Recent calculations of Sun *et al* [57] show that also the He–Cu interaction potential is anticorrugated.

To include mathematically in the He atom–surface interaction the effect of the anticorrugation we write the total potential as a sum of pairwise potentials of the form

$$V_i(\vec{r}) = \sum_{l,\kappa,\vec{b}\neq 0} v_a(\vec{r} - \vec{r}_{l\kappa} - \vec{u}_{l\kappa} - \vec{b}) \tag{46}$$

where the crystal atoms are in the ideal atomic positions and the $\vec{b}$ are the mid-positions of the neighbouring atoms, i.e. the centres of the bridge positions. By using equation (46) the dynamical interaction of equation (22) can be written as

$$\vec{F}_\kappa(\vec{Q}+\vec{G},z) = -S(\vec{Q}+\vec{G})\left(\mathrm{i}(\vec{Q}+\vec{G}),\frac{\partial}{\partial z}\right)v_a(\vec{Q}+\vec{G},z-z_\kappa)\mathrm{e}^{\mathrm{i}(\vec{Q}+\vec{G})\cdot\vec{r}_\kappa} \tag{47}$$

where

$$S(\vec{Q}+\vec{G}) = \sum_{\vec{b}\neq 0}\mathrm{e}^{\mathrm{i}(\vec{Q}+\vec{G})\cdot\vec{b}}. \tag{48}$$

5. Lattice dynamics

The theoretical development of the surface lattice dynamics from first principles is very difficult for metals, because of the screening of the ion–ion interaction by the conduction electrons in

the presence of a free surface. In the case of the noble and transition metals, because of the presence of the occupied d levels and the consequent sp–d electron hybridization, the difficulties increase. The phonon calculations are then usually based on Born–von Karman empirical force constant models [58–61], in which the force constants are obtained by least-squares fits of the bulk properties such as the bulk phonon spectrum and the elastic constants. At the surface and near the surface the force constants are treated as free parameters to reproduce the experimental surface phonon dispersion relations [29, 62]. The most accurate empirical model include not only force constants derived from pairwise interactions, but also force constants related to three-ion interactions [63]. The three-ion interactions mimic the effects of the electron gas screening and in the bulk are responsible for the violation of the Cauchy relations [64]. In the SE models, instead of using a semi-infinite crystal it is convenient to use the slab method first proposed by Allen *et al* [65]. In this way the surface is automatically included in the dynamical problem. Among the systems studied using this approach we mention the low-Miller-index surfaces of noble and transition metals such as Ag [62] and Pt [29] and of the simple metals such as Al [66].

Recently it has been possible to carry out first-principles calculations of surface force constants. The calculations have been performed for the simple sp metals Al and Na in the framework of the PP theory. Beatrice and Calandra [67] carried out a calculation to second order in the PP for the alkali metal surface phonons. The ground state and the response properties of the electronic subsystem were calculated in the infinite-barrier model for the electron wavefunctions.

An improvement of the theory has been given by Eguiluz *et al* [68] by evaluating self-consistently the electron response function. The wavefunctions were obtained by the self-consistent solution of the Kohn–Sham equations of density functional theory, by using the local density approximation for exchange and correlation. The response function was evaluated by treating the PP by second-order perturbation theory. A further improvement of this theory has been presented by Quong *et al* [69] by treating the PP exactly. The effects of the three-ion interactions are automatically included in this theory.

A different approach has been followed by Ho and Bohnen [70] by using the frozen-phonon method. These authors evaluate a few interlayer and intralayer force constants at the surface of Al(110) by creating the appropriate high-symmetry distortions of the outermost layers. The distortion energy is obtained with a total-energy PP calculation in the density functional theory. They calculate the phonon frequencies at high-symmetry points in the SBZ and they use a force constant model to fit these frequencies in order to obtain the dispersion relations in the whole SBZ.

A multipole expansion method has been used to study phonons in metals [71]. Following this method Benedek *et al* have extended the electron pseudocharge multipole expansion method [72] to construct an effective dynamical matrix for the surface vibrations of the Cu surfaces [71, 73].

The molecular dynamics approach has been applied to the study of the temperature dependence of phonons of model crystals [74], of W(001) [75], of Cu(110) [76], of Ni surfaces [77], of Al, Ni and Cu surfaces [78] and of Ag(110), Cu(001) and Ag(111) [79].

6. Comparison of the He atom scattering experiments with theory

We first discuss the simple metal case, illustrating the atom–surface scattering features of Al. For this system both SE and first-principles *ab initio* calculations of the phonon spectrum are available [66]. It is then possible to make a direct quantitative comparison between the two different approaches. In the SE model the crystal interatomic potential

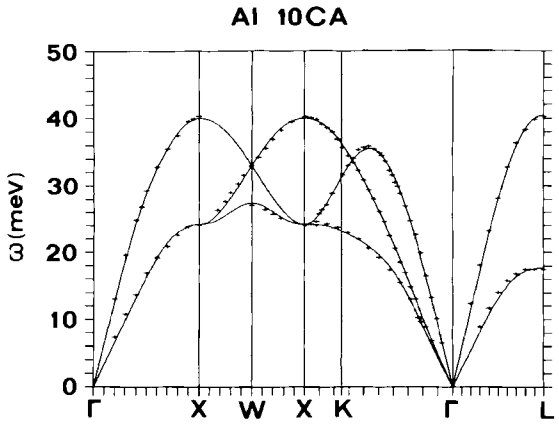

Figure 3. Bulk phonons of Al calculated along the symmetry directions of the Brillouin zone. The crosses represent the neutron experimental data of [80].

contains central two-body interactions V_c and angular-dependent three-body interactions V_a, parametrized by the tangential force constant $\alpha_i = (1/r)(\partial V_c/\partial r)|_{r=r_i}$, the radial force constant $\beta_i = (\partial^2 V_c/\partial r^2)\,|_{r=r_i}$ and the angular force constant $\delta_k = 1/3a_0^2\,(\partial^2 V_a/\partial \cos\theta^2|_{\theta=\theta_k}$, where r_i is the equilibrium distance from the atom at the origin of the ith shell of neighbours and θ_k is the angle formed by a triplet of atoms.

The values of the bulk force constants, as mentioned before in section 5, are obtained by a least-squares fit of the experimental bulk phonon spectrum and of the second-order elastic constants [59]. The quality of this fit is depicted in figure 3, where the bulk phonon dispersion relations calculated by taking into account a long-ranged up to ten nearest neighbours two-body potential and a short-ranged up to two nearest neighbours angular potential are drawn, compared with the experimental measurements with neutron scattering [80].

Similar results for bulk Al phonons are obtained with the *ab initio* PP theory of Eguiluz *et al* [68]. The values of the force constant tensors calculated with this first-principles approach are in quantitative agreement with those obtained in the SE model [64].

The surface phonon calculations for Al(111) are performed for a slab of 60 atomic planes in the SE approach, while in the *ab initio* case the calculations are made for a semi-infinite crystal [66]. In the SE model we obtain a very good agreement with the experimental measured phonon dispersion curves by taking into account a small increase (up to 2%) of the interplanar radial leading force constant, due to the surface relaxation of the outermost atomic plane.

In figure 4 we draw the calculated dispersion curves of the Rayleigh wave (RW) for two high-symmetry directions of the two-dimensional Brillouin zone and for two non-symmetry directions. The agreement with experimental He atom scattering data [21] is excellent for all these directions.

A typical TOF spectrum, corresponding to the scan curve for $E_i = 27.0$ meV, $\theta_i = 40.2^\circ$ and $\theta_f = 51.3^\circ$ is plotted in figure 5 together with the reflection coefficients evaluated using equations (26) and (47) with $S(Q) = 1$ in the SE model and in the PP model. This is in agreement with recent calculations of Sun *et al* [57] showing that the He–Al interaction potential is corrugated. The most prominent feature of the experimental histogram is the Rayleigh peak at $\omega_{RW} = -6$ meV. Because of its shape the scan curve intersects the RW mode twice in the TOF spectrum, yielding the second feature seen at $\omega_{RW} = -14.6$ meV. The RW mode is well reproduced by both the SE and the PP models.

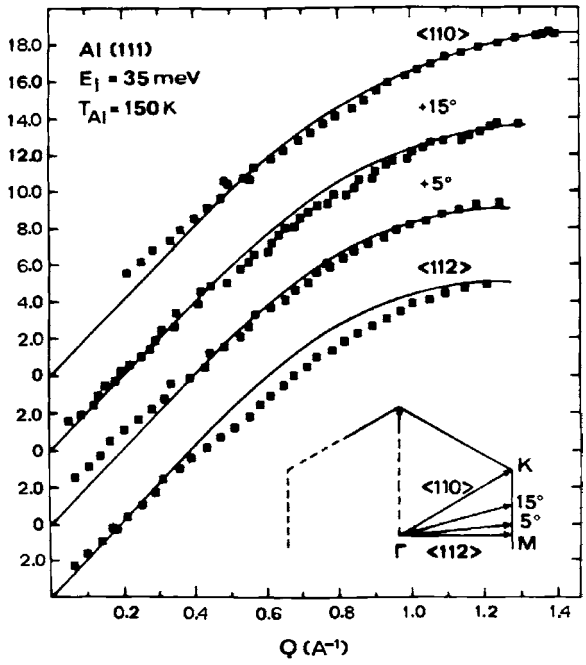

Figure 4. Dispersion relation of the RW of Al(111) along the four directions of the two-dimensional Brillouin zone shown in the inset. The squares are the He scattering experimental data of [21].

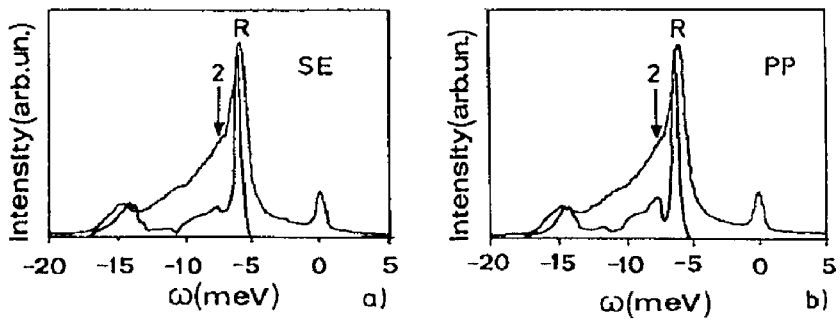

Figure 5. Comparison between experimental (histogram) and theoretical reflection coefficients of Al(111) for the scattering geometry indicated in the text. (*a*) refers to the SE calculations, while (*b*) refers to the PP *ab initio* calculations. R indicates the RW and 2 the LR [66].

In a similar way we have evaluated the reflection coefficients for several scattering geometries of Al(001) and in the diagrams of figure 6 we report the calculated dispersion of the maxima for the RW mode and for the other detectable peaks. The full curves correspond to the evaluated maxima, obtained from equation (26), and the circles are the maxima of the experimental TOF spectra [66]. The agreement between the two models is very good in the lower part of the dispersion curves. The comparison with the experimental data in this region is also extremely satisfactory. One notes a disagreement at higher phonon energies between the PP calculations and the experimental data for the weak resonance denoted by 1. We do not consider this to be a serious discrepancy if we recall that the *ab initio* PP calculations are based on second-order perturbation theory. The inclusion of third-order terms in the PP

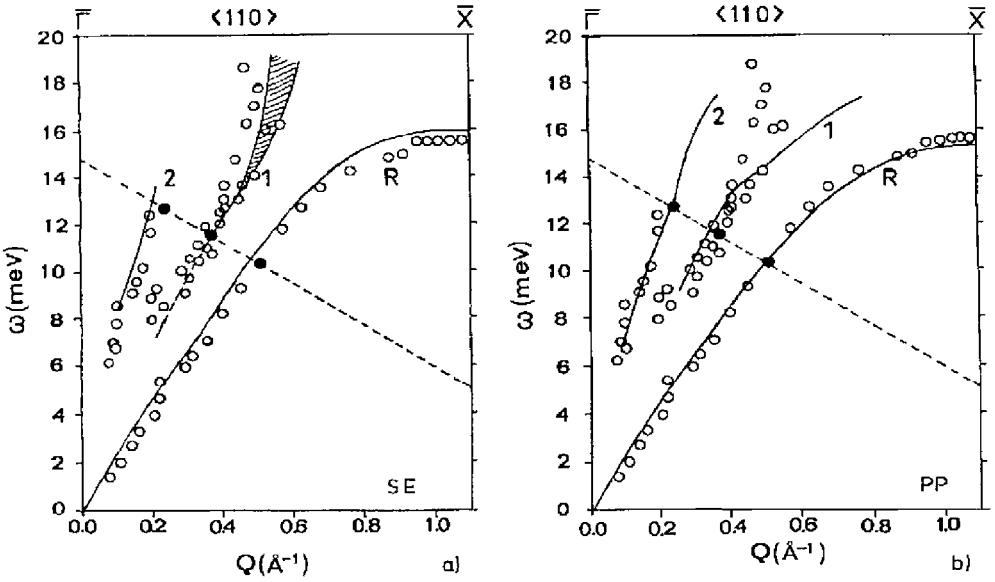

Figure 6. Dispersion relation of the phonon modes of Al(001) along the ⟨110⟩ symmetry direction of the two-dimensional Brillouin zone. Circles represent the He scattering experimental data [66].

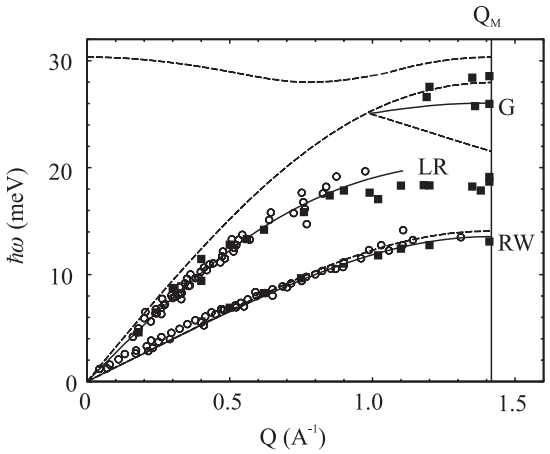

Figure 7. Dispersion relation of the phonon modes of Cu(111) with Q along the ⟨112⟩ direction of the two-dimensional Brillouin zone. Circles refer to HAS measurements [25]. Squares refer to EELS data [58].

in the evaluation of the total energy would probably be sufficient to eliminate these small discrepancies.

To discuss the noble and transition metal case, we illustrate now the Cu and Rh atom–surface scattering features. As mentioned before in section 4 for these metals the He–surface interaction potential is anticorrugated. First we show the results of the SE calculations for the Cu(111) surface [81]. To account for the charge redistribution occurring in the surface region we adjust the leading force constants by a trial-and-error procedure, starting with a

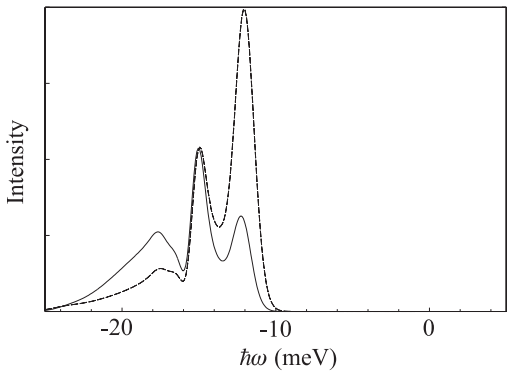

Figure 8. Reflection coefficient of Cu(111) with scattering geometry discussed in the text. The continuous curve is the full calculation, while the dashed curve is with $S(Q) = 1$.

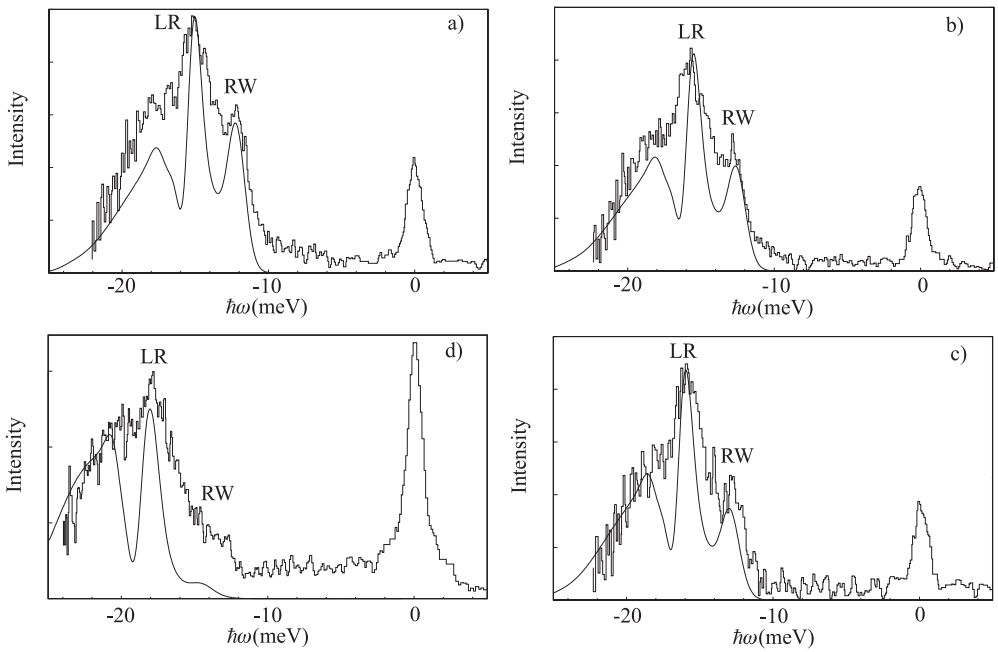

Figure 9. Comparison between measured TOF spectra [25] and calculated reflection coefficients for several scattering geometries for $E_i = 35.16$ meV: (*a*) $\theta_i = 33.5^\circ$, (*b*) $\theta_i = 33.0^\circ$, (*c*) $\theta_i = 32.5^\circ$ and (*d*) $\theta_i = 30.0^\circ$. The total scattering angle is $\theta_{sd} = 90.5^\circ$.

variation of the first-neighbour force constants. With this procedure we found that the in-plane tangential force constant $\alpha_1^{\parallel}$ is increased by 10%, giving rise to a surface stress, the in-plane radial $\beta_1^{\parallel}$ force constant is softened by about 16% and the interplanar radial force constant $\beta_1^{\perp}$ is stiffened by about 20%, while the angular force constant δ_1 is increased by 20%. These modest variations of the interactions are consistent with the PP calculations of Bohnen *et al* [83] for the Cu(111) surface. Figure 7 shows the calculated dispersion curves in the $\bar{\Gamma}\bar{M}$ direction. The full curves indicate the Rayleigh branch, the longitudinal resonance (LR) and the gap mode (G). The dashed curves correspond to the edges of the projected bulk bands. Circles

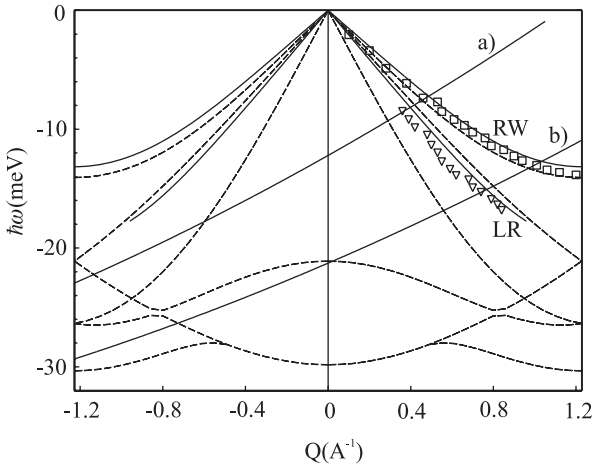

Figure 10. Dispersion relation of the phonon modes of Cu(001) with Q along the $\langle 110 \rangle$ direction. Squares and triangles refer to the experimental HAS data [30] and EELS data [84]. Two typical scan curves are also drawn for $E_i = 39.9$ meV: (*a*) $\theta_i = 40.0^\circ$ and (*b*) $\theta_i = 34.5^\circ$.

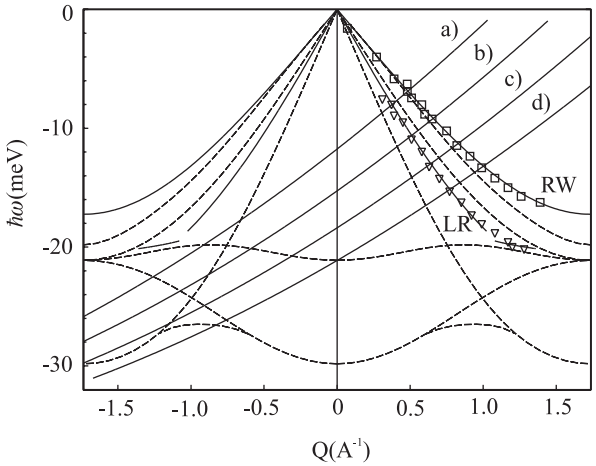

Figure 11. Dispersion relation of the phonon modes of Cu(001) with Q along the $\langle 100 \rangle$ direction. Squares and triangles refer to the experimental HAS data [30]. The scan curves drawn in the figure refer to the TOF spectra of figure 12.

represent the He scattering data [25], while the squares refer to the EELS measurements [58]. In figure 8 is shown the reflection coefficient evaluated with equation (26) in the $\langle 11\bar{2} \rangle$ direction with and without the structure factor of equation (48) for $E_i = 35.16$ meV, $\theta_i = 33.5^\circ$ and $\theta_f = 66.5^\circ$. The dashed curve refers to $S(\boldsymbol{Q}) = 1$. One notices that at large negative energy transfer the two spectra coincide. This region corresponds to bulk projected on the surface with small momentum transfer along the scan curve (depicted in figure 7). One notes a strong reduction of the LR intensity and an even stronger reduction of the RW intensity in the region of large momentum transfer. The structure factor, which is a function rapidly decreasing with increasing momentum, has the effect of reducing in a dramatic way the height of the RW peak with respect to the height of the LR, in agreement with the experimental findings. In figure 9 are drawn several spectra as a function of θ_i (see the caption of figure 9 for details). By decreasing

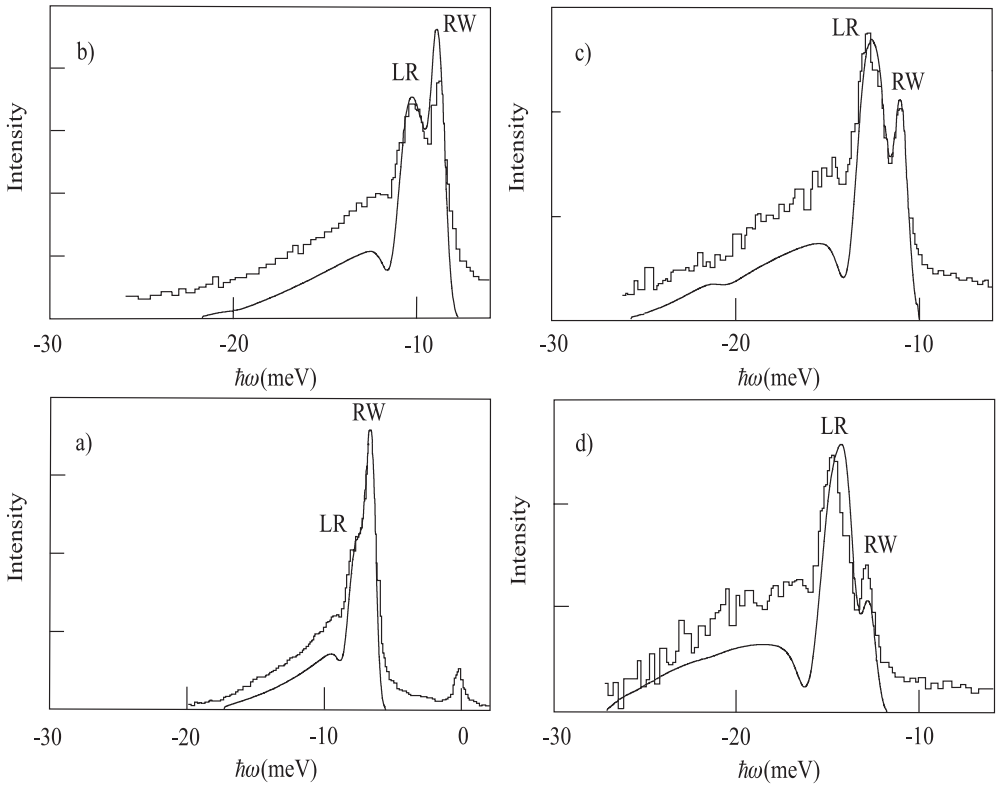

Figure 12. Comparison between TOF spectra [30] (histogram) and evaluated reflection coefficients for Cu(001) with Q along the ⟨100⟩ direction for several scattering geometries at $E_i = 34.4$ meV: (*a*) $\theta_i = 40.0^\circ$, (*b*) $\theta_i = 38.0^\circ$, (*c*) $\theta_i = 36.0^\circ$ and (*d*) $\theta_i = 34.0^\circ$.

θ_i the momentum transfer of the RW is rapidly increasing and the structure factor is rapidly decaying on this mode. Furthermore the structure factor does not affect the bulk projected continuum around -20 meV, because these projected phonons have small lateral momentum. As one can see the anticorrugation effect not only gives the reason for the overtaking of the intensity of the LR with respect to the Rayleigh mode, but also explains in terms of bulk projected phonons the large structure observed in the spectra located around -20 meV. For the geometry $\theta_i = 30^\circ$ where $Q_{RW} = 1.45$ Å^{-1} and $Q_{LR} = 0.88$ Å^{-1} the decay of the structure factor is so strong that only the LR is observed in agreement with the experiments.

The non-close-packed (001) surface of Cu is even more interesting [81] than the (111) surface. For this surface there has been found experimentally [30] a giant LR which is strongly anisotropic with its maximum intensity along the ⟨100⟩ direction. The surface lattice model is constructed as for the (111) surface. In this case we obtain modest variation of the surface force constants: a surface tensile stress of 10%, a reduction of 12% for $\beta_1^{\parallel}$ and an increase of 20% of the interplanar $\beta_1^{\perp}$. The last value agrees with the theoretical calculations of Chen *et al* [84]. The evaluated surface phonon frequencies together with the atom scattering [30] and EELS data [84] are reported in figure 10 for a Q along the ⟨011⟩ direction and in figure 11 for Q along the ⟨001⟩ direction. The full curves are the evaluated Rayleigh and longitudinal LR branches. Dashed curves are the edges of the bulk projected phonons. In the calculated reflection coefficients shown in figure 12 one sees clearly that decreasing θ_i, i.e. increasing the

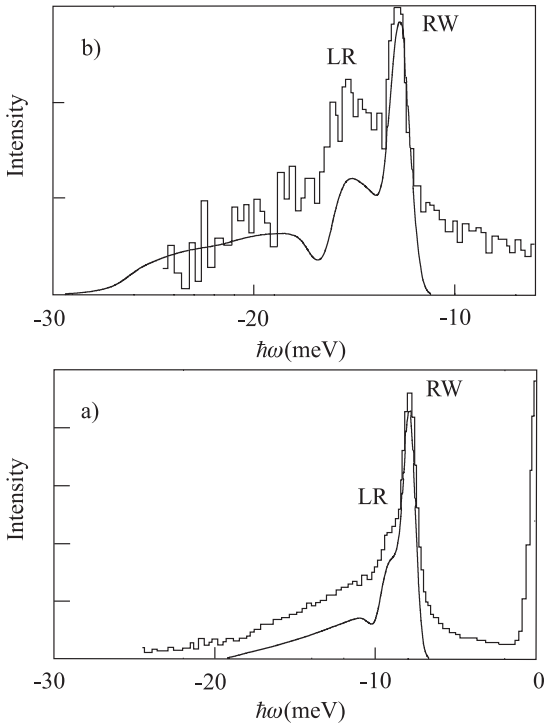

Figure 13. Comparison between TOF spectra [30] (histogram) and evaluated reflection coefficients for Cu(001) with Q along the ⟨110⟩ direction for two scattering geometries at $E_i = 39.9$ meV: (*a*) $\theta_i = 40.0^\circ$ and (*b*) $\theta_i = 34.5^\circ$.

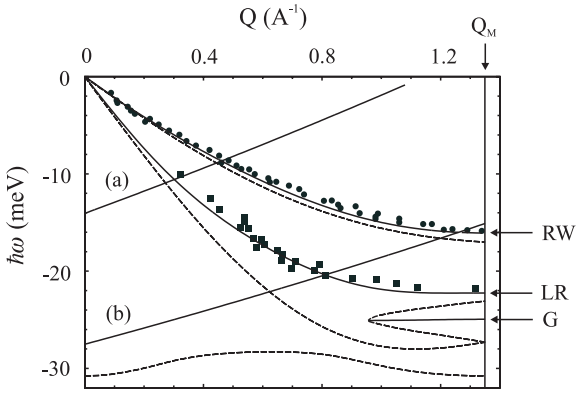

Figure 14. Surface phonon frequencies of Rh(111) with Q along the ⟨112⟩ surface symmetry direction. The dashed curves correspond to bulk projected phonons, while the full curves refer to the surface phonon modes. Dots and squares are the HAS data from [31]. Curves (a) and (b) are the scan curves for $\theta_i = 40.5^\circ$ and $\theta_i = 34.0^\circ$ respectively.

lateral momentum, the LR overtakes the RW mode and resembles a huge resonance. Note that in the region $(-20, -10)$ meV the contribution of the projected bulk phonon in our reflection coefficients reproduces quite well the behaviour of the spectra. The calculated spectra along the ⟨011⟩ direction are presented in figure 13. One sees that the height of the RW mode is

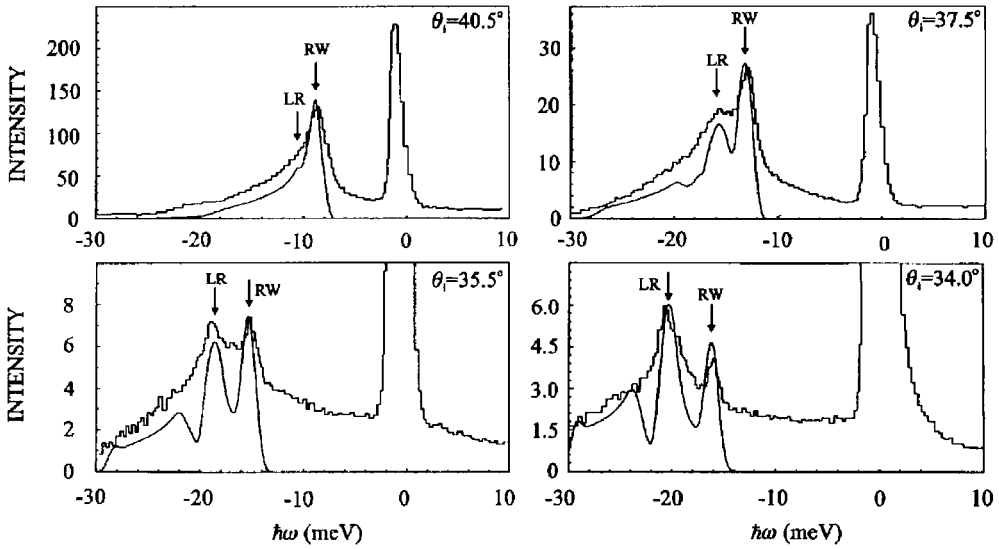

Figure 15. Comparison between measured TOF spectra [31] and the evaluated reflection coefficients of Rh(111) for several scattering geometries indicated in the figure.

clearly higher than that of the LR. This is due to the structure factor, that in this direction does not decay rapidly enough to reduce the RW mode intensity.

To evaluate the surface phonons of Rh(111) we have chosen [82] an SE interatomic potential in which the bulk interactions are central long ranged up to ten nearest neighbours and non-central up to two nearest neighbours, with modifications of the leading surface force constants by about 20% with respect to their bulk values, in agreement with *ab initio* calculations [85].

In figure 14 are drawn the dispersion relations of the RW, the LR and the gap mode for Q along the ΓM direction of the 2DBZ, along with two typical scan curves of the He scattering experiments. Circles and squares refer to the measurements of [31]. The dashed curves represent the edge of bulk phonons projected onto the surface. As one can see the agreement between theory and experiments is excellent.

In figure 15 are drawn the experimental [31] (histogram) and theoretical (full curve) TOF spectra calculated with equation (26) by taking into account the anticorrugating function of equation (48), for four different scattering geometries (see the caption for details). As one can see, the ratio of scattering intensity of the RW with respect to that of the LR decreases on increasing the energy and momentum transfer, in agreement with the experiments. In the spectrum taken at $\theta_i = 34°$, relative to the scan curve (b) of figure 14, the LR intensity overtakes that of the RW, while the structure observed between $\omega = -30$ and -25 meV is relative to scattering from bulk phonons. In conclusion, the anticorrugating effect fully explains the anomalous height of the LR observed by He scattering. As Q increases, the structure factor decreases the height of the RW peak, and at large momentum the LR intensity overtakes the RW intensity.

References

[1] Stern O 1929 *Naturwissenschaften* **17** 391
[2] Jackson J M and Mott N F 1932 *Proc. R. Soc.* A **137** 703

[3] Boato G and Cantini P 1983 *Advances in Electronics and Electron Physics* vol 60, ed P W Hawks (New York: Academic) p 25
[4] Doak R B 1981 *PhD Thesis* Massachusetts Institute of Technology *Max Planck fur Stromungsforschung Bericht* 14/1981 (Goettingen)
[5] Benedek G and Valbusa U 1982 *Dynamics of Gas–Surface Interaction* (Berlin: Springer)
[6] Goodman F O and Wachman H Y 1976 *Dynamics of Gas–Surface Scattering* (New York: Academic)
[7] Engel T and Rieder K H 1982 *Structural Studies of Surfaces* ed G Hohler (Berlin: Springer) p 55
[8] Toennies J P 1984 *J. Vac. Sci. Technol.* A **2** 1055
[9] Celli V 1984 *Many-Body Phenomena at Surfaces* ed D Langreth and H Suhl (Orlando, FL: Academic) p 315
[10] Barker J A and Auerbach D J 1985 *Surf. Sci. Rep.* **4** 1
[11] Bortolani V and Levi A C 1986 *Riv. Nuovo Cimento* **9** 1
[12] Gumhalter B 2001 *Phys. Rep.* **351** 1
[13] Brusdeylins G, Doak R B and Toennies J P 1981 *Phys. Rev. Lett.* **46** 437
[14] Bracco G, Tatatrek R, Terreni S and Tommasini F 1986 *Phys. Rev.* B **34** 9045
[15] Brusdeylins G, Doak R B and Toennies J P 1983 *Phys. Rev.* B **27** 3662
[16] Benedek G, Brusdeylins G, Doak R B, Skofronick J G and Toennies J P 1983 *Phys. Rev.* B **28** 2104
[17] Harten U and Toennies J P 1987 *Europhys. Lett.* **4** 833
[18] Ernst H J and Hulpke E 1987 *J. Vac. Sci. Technol.* A **5** 460
[19] Brusdeylins G, Rechsteiner R, Skofronick J G, Toennies J P, Benedek G and Miglio L 1986 *Phys. Rev.* B **34** 902
[20] Harten U, Toennies J P and Wöll Ch 1986 *Phys. Rev. Lett.* **57** 2947
[21] Lock A, Toennies J P, Wöll Ch, Bortolani V, Franchini A and Santoro G 1988 *Phys. Rev.* B **37** 7087
[22] Toennies J P and Wöll Ch 1987 *Phys. Rev.* B **36** 4475
[23] Doak R B, Harten U and Toennies J P 1983 *Phys. Rev. Lett.* **51** 578
[24] Bracco G, Tatarek R, Tommasini F, Linke U and Persson M 1987 *Phys. Rev.* B **36** 2928
[25] Harten U, Toennies J P and Wöll Ch 1985 *Faraday Discuss. Chem. Soc.* **80** 137
[26] Cates M and Miller D R 1983 *Phys. Rev.* B **28** 3615
[27] Lahee A M, Toennies J P, Wöll Ch, Bohnen K P and Ho K M 1989 *Europhys. Lett.* **10** 261
[28] Mason B F, McGreer K and Williams B R 1983 *Surf. Sci.* **130** 282
[29] Bortolani V, Franchini A, Santoro G, Toennies J P, Wöll Ch and Zhang G 1989 *Phys. Rev.* B **40** 3524
[30] Benedek G, Ellis J, Luo N S, Reichmuth A, Ruggerone P and Toennies J P 1993 *Phys. Rev.* B **48** 4917
[31] Witte G, Toennies J P and Wöll Ch 1995 *Surf. Sci.* **323** 228
[32] Gell-Mann M and Goldberger M L 1953 *Phys. Rev.* **91** 398
[33] Cabrera N, Celli V and Manson R 1969 *Phys. Rev. Lett.* **22** 346
Manson R and Celli V 1971 *Surf. Sci.* **24** 495
[34] Aziz R A 1984 *Inert Gases* ed M L Klein (Berlin: Springer)
[35] Tang K T and Toennies J P 1984 *J. Chem. Phys.* **80** 3726
[36] Norskov J K and Lang N D 1980 *Phys. Rev.* B **21** 2131
[37] Stott M J and Zaremba E 1980 *Phys. Rev.* B **22** 1564
[38] Norlander P and Harris J 1984 *J. Phys. C: Solid State Phys.* **17** 1141
[39] Manninen M, Norskov J K, Puska M J and Umrigar C 1984 *Phys. Rev.* B **29** 2314
[40] Takada Y and Kohn W 1987 *Phys. Rev.* B **37** 826
[41] Esbjerg N and Norskov J K 1980 *Phys. Rev. Lett.* **45** 807
[42] Batra I P, Bagus P S and Barker J A 1985 *Phys. Rev.* B **31** 1737
[43] Harris J and Liebsch A 1982 *J. Phys. C: Solid State Phys.* **15** 2275
[44] Lifshitz E M 1956 *Sov. Phys.* **2** 73
[45] Zaremba E and Kohn W 1976 *Phys. Rev.* B **13** 2270
[46] Zaremba E and Kohn W 1977 *Phys. Rev.* B **15** 1769
[47] Zaremba E and Kohn W 1982 *Phys. Rev.* A **25** 782
[48] Vidali G, Ihm G, Kim H-Y and Cole M W 1991 *Surf. Sci. Rep.* **12**
[49] Hill N R, Haller M and Celli V 1982 *Chem. Phys.* **73** 363
[50] Eichenauer D, Harten U, Toennies J P and Celli V 1987 *J. Chem. Phys.* **86** 3693
[51] Dondi M G, Terreni S, Tommasini F and Linke U 1988 *Phys. Rev.* B **37** 8034
[52] Tersoff J 1985 *Phys. Rev. Lett.* **55** 140C
[53] Rieder K H, Parschau G and Burg B 1993 *Phys. Rev. Lett.* **71** 1059
[54] Rieder K H and Garcia N 1982 *Phys. Rev. Lett.* **49** 43
[55] Annett J F and Haydock R 1984 *Phys. Rev. Lett.* **53** 838
[56] Petersen M, Wilke S, Ruggerone P, Kohler B and Scheffler M 1996 *Phys. Rev. Lett.* **76** 995
[57] Qjang Sun at press

[58] Lewhald S, Szeftel J M, Ibach H, Rahman T S and Mills D L 1983 *Phys. Rev. Lett.* **50** 518
[59] Bortolani V, Franchini A, Nizzoli F and Santoro G 1985 *Electronic Structure, Dynamics and Quantum Structural Properties of Condensed Matter* ed J T Devreese and P Van Camp (New York: Plenum) p 401
[60] Black J E, Campbell D A and Wallis R F 1982 *Surf. Sci.* **115** 161
[61] Black J E, Franchini A, Bortolani V, Santoro G and Wallis R F 1987 *Phys. Rev.* B **36** 2996
[62] Bortolani V, Franchini A, Nizzoli F and Santoro G 1984 *Phys. Rev. Lett.* **52** 429
[63] Clark B C, Gazis D C and Wallis R F 1964 *Phys. Rev.* A **134** 1486
[64] Wallis R F, Maradudin A A, Bortolani V, Eguiluz A G, Franchini A and Santoro G 1993 *Phys. Rev.* B **48** 6043
[65] Allen R E, Alldredge G P and de Wette F W 1971 *Phys. Rev.* B **4** 1648
[66] Franchini A, Bortolani V, Santoro G, Celli V, Eguiluz A G, Gaspar J A, Gester M, Lock A and Toennies J P 1993 *Phys. Rev.* B **47** 4691
[67] Beatrice C and Calandra C 1983 *Phys. Rev.* B **28** 6130
[68] Eguiluz A G, Maradudin A A and Wallis R F 1988 *Phys. Rev. Lett.* **60** 309
[69] Quong A A, Maradudin A A, Wallis R F, Gaspar J A, Eguiluz A G and Alldredge G P 1991 *Phys. Rev.* **66** 743
[70] Ho K M and Bohnen K P 1986 *Phys. Rev. Lett.* **56** 934
[71] Jayanthi C S, Bilz H, Kress W and Benedek G 1987 *Phys. Rev. Lett.* **59** 795
[72] Allen P B 1977 *Phys. Rev.* B **16** 5139
[73] Kaden C, Ruggerone P, Toennies J P, Zhang G and Benedek G 1992 *Phys. Rev.* B **46** 13 509
[74] McGurn A R, Maradudin A A, Wallis R F and Ladd A J 1988 *Phys. Rev.* B **37** 3964
[75] Wang C Z, Fasolino A and Tosatti E 1988 *Phys. Rev.* B **37** 2116
[76] Ditlevson P D, Stolze P and Norskov J K 1991 *Phys. Rev.* B **44** 13 002
[77] Beaudet Y, Lewis L J and Persson M 1994 *Phys. Rev.* B **50** 12 084
[78] Ditlevson P D and Norskov J K 1991 *Surf. Sci.* **254** 261
[79] Yang L, Rahman T S and Daw M S 1991 *Phys. Rev.* B **44** 13 725
Al-Rawwi A N, Kara A and Rahman T S 2000 *Surf. Sci.* **446** 17
[80] Stedman R and Nilsson G 1966 *Phys. Rev.* **145** 492
[81] Santoro G, Franchini A, Bortolani V, Mills D L and Wallis R F 2001 *Surf. Sci.* **478** 99
[82] Santoro G, Franchini A and Bortolani V 1998 *Phys. Rev. Lett.* 80 2378
[83] Chen Y, Tong S Y, Bohnen K P, Rodach T and Ho K M 1993 *Phys. Rev. Lett.* **70** 603
[84] Chen Y, Tong S Y, Jae-Sung Kim, Kesmodel L L, Rodach T, Bohnen K P and Ho K M 1991 *Phys. Rev.* B **44** 11 394
[85] Eichler A, Bohnen K P, Reichardt W and Hafner J 1998 *Phys. Rev.* B **57** 324